Supporting Information

Küpper *et al.* 10.1073/pnas.0709959105

SI Text

The following contains further results, experimental and theoretical datasets, and elements of discussion, including a range of control experiments. In the XAS studies, freeze-dried *Laminaria* was compared with fresh tissues, flash-frozen in liquid nitrogen, to study the role of biological compartments in iodine accumulation. L_3-edge XAS was conducted as a control to corroborate the key findings of K-edge XAS reported above. Our studies of iodine uptake and efflux had started by measuring iodine fluxes with ^{125}I-labeled iodine, before studying the chemical speciation. Following the finding of iodide as the accumulated species, toxicity experiments were carried out on both prokaryotic and eukaryotic cells to verify any potential, more directly defense-related role. Next, detailed calculations of ozone deposition velocity on *Laminaria* thallus surfaces and molecular iodine, iodocarbon, and particle emission rates are reported. Finally, we present a synopsis of thermodynamic and kinetic data highlighting the favorable properties of iodide (also as opposed to bromide or chloride) as antioxidant.

Materials and Methods

Iodine Speciation in Seawater Surrounding Laminaria. Iodide was determined by cathodic stripping square wave voltammetry (CSSWV) (1). The scan was from −0.15 to −0.90 V, with deposition potential of −0.15 V vs. Standard Calomel Electrode (SCE), deposition time 30 s, equilibration time 5 s, scan rate 200 $mV{\cdot}s^{-1}$, pulse height 20 mV. The iodide wave appeared at −0.33 V. The optimum linear range of the method for algal culture media as used here was up to 0.2 μM: appropriate sample dilutions were performed in 0.7 M NaCl, adjusted to pH 8 with $NaHCO_3$. Calibration was done by standard additions (1). Iodate was determined by linear sweep voltammetry (LSV), an adaptation of the differential pulse polarography method (2). The scan was from −0.8 V to −1.5 V vs. SCE. Using a scan rate of 1 $V{\cdot}s^{-1}$, the iodate wave appeared at −1.28 V. Detection limit with these conditions was 0.5 μM, with a linear range of up to at least 25 μM, using KIO_3 standards prepared in 0.7 M $NaCl/NaHCO_3$, pH 8. Dissolved organic iodine was determined via hypochlorite oxidation (3), whereby all dissolved iodine forms are oxidized to iodate. Total dissolved iodine (I_{ox}) was determined by LSV as above, then any organic iodine present was calculated by subtraction of iodide and iodate concentrations from total I_{ox}. Precision for both iodide by CSSWV and iodate by LSV was better than 5%.

Ozone Scavenging and Particle Formation Experiments. Experiments were conducted in a special glass flow reactor, under 1.7 l min^{-1} of BOC zero grade air. *L. digitata* was collected from the west coast of Scotland and incubated at 3°C in the dark with continuous aeration until required for experiments (or freeze-dried, respectively). Measured, weighed, and towel-dried strips of fresh or freeze-dried *Laminaria* (with surface areas ranging from 20 to 200 cm^2) were placed in a 2-liter primary chamber. Downstream, a second 2-liter chamber provided an increase (of 1.2 min) in the residence time, allowing particle-forming reactions to occur. The total mean residence time from the first chamber to the particle counter was ≈4 min. The flow reactor was kept either dark or exposed to UV-vis radiation from four 350-W Sylvania Blacklight (Philips) bulbs with an emission maximum at 350 nm (and very little emission above 405 nm). The photolysis lifetime of I_2 in the irradiated flow reactor system was measured as 10 min.

Ozone came from an adjustable ozone generator (PenRay model SOG-2) and was measured from before and after the primary chamber using a UV absorption-based 2B 202 ozone monitor. Aerosol particles were measured with a condensation particle counter (CPC) TSI model 3025 (diameters >3 nm).

Formation of Molecular Iodine During Ozone Exposure of *Laminaria thalli*. I_2 in the gas phase was trapped by bubbling through a 50-cm^3 ethanol trap and quantified as I^- (absorbance band at 225 nm) using a UV/vis absorption spectrometer (Shimadzu PharmaSpec 1700) calibrated with standard solutions. The stripping efficiency for I_2 was determined as 100% at the relevant concentrations by passing the exhaust of the trap through a secondary ethanol trap. In alkaline solution, I_2 disproportionates rapidly, with iodide as the dominant product:

$$3I_2 + 6OH^- \rightarrow 5I^- + IO_3^- + 3H_2O.$$

Also, any gas phase HOI and HI released will be measured by this indirect detection method.

Halocarbon Measurements. Volatile chloro-, bromo-, and iodocarbons were measured by using a PerkinElmer Turbomass electron ionization GC-MS in selective ion recording mode. Separation was achieved using a DB5 625 capillary column (30 m × 0.32 mm internal diameter) with CP grade helium carrier gas. Sample volumes of 1.5 liters were preconcentrated on an adsorbent trap (Air Toxics) held at −30°C before being transferred to the GC by rapid heating to 300°C, using a PerkinElmer TurboMatrix Automated Thermal Desorption unit (ATD). Detection limits were between 0.02 and 0.12 pptv for approximately hourly samples of $CHCl_3$, CH_3I, C_2H_5I, n-C_3H_7I, i-C_3H_7I, CH_2ClI, CH_2Br_2, $CHBr_2Cl$, CH_2BrI, $CHBr_3$, and CH_2I_2 with a precision of 3–8% and complete recovery of all compounds. Any variability in instrument sensitivity between samples was accounted for using a National Physics Laboratory (NPL) external standard and calibration was achieved by using the output from dynamically diluted, thermostatic permeation tubes.

Bacterial Growth Assay. To test for toxic effects of iodide on a kelp epiphyte, a growth assay with the bacterial strain Ldm2 was carried out as described in ref. 4 in the presence of 10^{-5}, 10^{-4}, 10^{-3}, 10^{-2}, and 10^{-1} M KI and a control without added iodide (18°C).

Vitality Assay for Human Leukocytes by Flow Cytometry. Possible toxic effects of iodide (1, 10, and 100 mM, respectively), bromide (10 mM), and iodate (50 mM) to human blood cells were investigated by flow cytometric detection of mitochondrial membrane potential. Isolated human leukocytes (5) were stained with 5 nM tetramethylrhodamine ethyl ester (TMRE) (Molecular Probes) for 10 min at 37°C and then washed once with PBS; cells were analyzed in a BD LSR flow cytometer (Becton Dickinson).

Determination of Glutathione. Total glutathione (GSH plus GSSG) in *Laminaria* tissues was quantified as described in ref. 6. Briefly, tissue samples were homogenized in lysis buffer (10 mM EDTA, 100 mM HCl). The precipitated proteins were removed by centrifugation. The supernatants and standards (0–5 μM GSSG) were further diluted in lysis buffer, and total glutathione was quantified with an ACP 5040 analyzer (Eppendorf) with two buffer systems: buffer A (pH 7.2) with 9 mM

EDTA, 180 mM KH_2PO_4, 120 mg·liter^{-1} BSA, and 360 μM 5,5′-dithiobis(2-nitrobenzoic acid), and buffer B (pH 7.2) with 1.5 mM EDTA, 75.2 mM imidazole, and 150 mg·liter^{-1} BSA; 2-nitro-5-thiobenzoic acid resulting from GSH oxidation was determined at 412 nm.

Determination of Ascorbate. Ascorbate was quantified as described (7), with minor modifications. Frozen algal tissue (150 mg) was ground in liquid nitrogen. After thawing and addition of 1 ml of 1 M $HClO_4$, two 50-μl aliquots were taken for the chlorophyll/pheophytin assay; the rest was centrifuged (15 min, 4°C). Thereafter, 500 μl of the supernatant was transferred to an ice-cooled, 2-ml Eppendorf cup containing 100 μl of 0.12 M NaH_2PO_4 (pH 5.6) and 130 μl of 2.5 M K_2CO_3, to adjust the pH to 5–6. Insoluble $KClO_4$ was removed by centrifugation (3 min at 25,000 × *g* and 4°C). Reduced ascorbate was determined photometrically at 265 nm (7). Final amounts of ascorbate were related to fresh weight (FW) (not to pheophytin).

Whole-Blood Assay for Determining the Antioxidant Potential of Iodide. As described in ref. 5, blood was withdrawn from healthy volunteers in Heparin monovettes (Sarstedt) and washed five times with phosphate buffer saline (PBS) (pH 7.4) to remove plasma. Hereafter, blood cells were resuspended in PBS to the original volume. Blood samples were then incubated for 30 min at 37°C with different concentrations (0.10–100 mM) of KI or KBr (Sigma). Then, an oxidative burst was stimulated with 2 μg·ml^{-1} phorbol 12-myristate 13-acetate (Sigma). After 5 min at 37°C, samples were centrifuged at 500 × *g* for 5 min and H_2O_2 was analyzed colorimetrically in the supernatants; 100 μl of Fox solution (0.1 mM xylenol orange, 0.25 mM ammonium ferrous sulfate, 100 mM sorbitol, 25 mM H_2SO_4) was mixed with 50 μl of supernatant and incubated at room temperature for 30 min, then optical density was measured at 550 nm. A standard curve was prepared with hydrogen peroxide. IC_{50} values were calculated from the raw data with the sigmoidal dose–response curve fit option in GraphPad Prism Software.

Results and Discussion

Iodine XAS. ***K-edge XAS of lyophilized* Laminaria.** Fig. 1 and Fig. S1 show the effects of lyophilization and rehydration of *Laminaria* phylloids on the iodine x-ray absorption spectra. The spectrum of lyophilized material is similar to that of fresh thalli, and the results of the refined simulations of the EXAFS are also similar (Table S1, 2.2 O at 3.51 Å vs. 1.6 O at 3.58 Å). This further supports that molecules other than water, such as carbohydrates, polyphenols, and/or proteins, likely provide the oxygen (or nitrogen) atoms that are detected in the iodine environment. The amplitude of the EXAFS and the main peak in the Fourier transform increase markedly upon rehydration in seawater (3.0 O at 3.42 Å; not shown). Furthermore, an unprecedented spectrum (Fig. 1 and Fig. S1) is obtained when the lyophilized phylloids are rehydrated in the presence of 2 mM H_2O_2 [a concentration similar to that occurring at the *Laminaria* thallus surface during an oxidative burst (4)]. A number of oscillations are now observed in the EXAFS while the Fourier transform shows atoms in the range of covalent bonds at ≈2 Å together with a strong shell at 3 Å, i.e., a combination of peaks that is characteristic of iodine bound to aromatic rings, such as in 3-iodotyrosine and 3,5-di-iodotyrosine (8). The spectrum could be simulated with a phenyl ring using the same multiple scattering approach used in our model compound study (8), and the distance of 2.09 Å is close to that identified as characteristic for a bond between iodine and sp^2-hybridized carbon in the earlier work. The virtually complete incorporation of iodine in aromatic groups under the influence of H_2O_2 is almost certainly catalyzed by the presence of haloperoxidases, which are capable of tyrosine iodination (9), among many other reactions (10, 11). The obvious explanation is that the lyophilization has disrupted parts of the ultrastructural cellular organization, so that exogenous hydrogen peroxide can penetrate cellular compartments in an unhindered manner and react with stored iodide and other cellular contents (e.g., polyphenols or phenylalanine- and tyrosine-rich proteins), catalyzed by haloperoxidases—which would not be the case under structurally ordered, physiological circumstances. Clearly, this is fundamentally different from the situation where fresh *Laminaria* phylloids are subjected to oxidative stress with oligoguluronates or H_2O_2, which only results in iodide and iodocarbon efflux (4, 12, 13). It should also be noted that the results obtained with lyophilized, H_2O_2-treated *Laminaria* tissues effectively simulate a (hypothetical) situation of a biological iodine pool largely bound to organic/aromatic residues.

L_3-edge XAS. The presence of iodide as the principal, accumulated form of iodine in *Laminaria* was further corroborated by I L_3-edge XANES. Studies at this absorption edge were conducted on a suitable set of model compounds and unstressed *Laminaria* tissues. The spectra of *Laminaria* and aqueous 10 mM NaI are identical in the edge position and shape (Fig. S2) and in stark difference to the spectra of $NaIO_3$ aq, $NaIO_4$ aq, iodotyrosine, iodoform, I_2, and CI_4 (not shown), all of which show different XANES pattern. The EXAFS amplitude for the *Laminaria* sample was very small, which is in line with the K-edge results.

Total Iodine Efflux Upon Oxidative Stress. Both GG and H_2O_2 induced a strong efflux of ^{125}I-labeled total iodine from *Laminaria* thalli (at a biomass density of 50 mg FW·ml^{-1}) that had been precharged for 48 h in seawater containing 23 Bq·ml^{-1} $Na^{125}I$ (all experimental details as described in ref. 14). The total amount of iodine released upon either an oxidative burst induced by 150 μg·ml^{-1} GG or treatment with 2 mM exogenous H_2O_2 was similar, albeit there were differences in kinetics: GG treatment resulted in a steady efflux over approximately 3 h after treatment, whereas the iodine efflux response to exogenous H_2O_2 treatment was much faster; i.e., within a few minutes after the onset (Fig. S3).

Iodine Speciation. Total iodine in seawater was 0.45 μM before oxidative stress, with iodate and iodide about equal in concentration. Although iodide concentrations of up to 64 μM were observed in the seawater surrounding *L. digitata* thalli after oxidative stress triggered by oligoguluronates, no significant changes of the iodate concentration compared with background levels were observed. Likewise, there was no measurable increase in organic iodine after oxidative stress (not shown).

Vitality Assay for a *Laminaria*-Associated Bacterial Strain. Potassium iodide had no significant effect on the growth of an epiphytic marine bacterium (Ldm 2) up to concentrations of over 10 mM. Only at the highest tested concentration, 100 mM, a 38% reduction in growth was observed in the exponential growth phase at 6 h after inoculation, which gradually reduced to <20% once the stationary phase was reached (Fig. S4).

Vitality Assay for Human Leukocytes by Flow Cytometry. To exclude possible cytotoxic effects of iodide, human leukocytes were stained with TMRE and measured with flow cytometry. Driven by the mitochondrial membrane potential, TMRE accumulates in mitochondria. Cytotoxic effects can be monitored by a reduced TMRE staining of cells resulting from an impaired mitochondrial membrane potential. Incubation with iodide for up to 1 h at 37°C showed that even high concentrations of 10 mM iodide showed no toxic effect on leukocytes. One hundred millimolar iodide was not toxic to leukocytes after a 20-min incubation. After a 1-h incubation, 100 mM iodide showed mild cytotoxicity (25% of cells with reduced mitochondrial membrane potential). Furthermore, part of the cells were incubated with

propidium iodide, a dye that stains DNA of dead or damaged cells but that is impermeable to viable cells with an intact cell membrane. A flow cytometric analysis of this staining showed that incubation for 1 h with iodide concentrations of up to 100 mM did not impair leukocyte viability.

Production of Molecular Iodine and Particles. Production of molecular iodine occurred at rates 2–3 orders of magnitude faster than iodocarbon production. The quantity of I_2 produced by *Laminaria* showed a relationship with the total particle numbers formed, whereas the iodocarbon concentration did not (Table S2).

Calculation of Theoretical Ozone Deposition Velocity. The total deposition velocity, v_D, is equal to $1/(r_a + r_l)$, where r_a is the aerodynamic resistance and r_l is the liquid phase resistance. The theoretical ozone deposition velocity due only to liquid phase diffusion and chemical reactions on the surface of *Laminaria* containing 20 mM I^- was calculated from $1/r_l = \sqrt{\lambda D/H}$ (15), where λ is the chemical loss rate of O_3 in seawater ($k_i[I^-]$, where k_i represents the second-order rate constant for the reaction of I^- with O_3), D is the molecular diffusivity of ozone in water (1.2×10^{-5} cm^2·s^{-1} at 20°C), and H is the dimensionless Henry's law constant ($H \equiv C_g/C_w \sim 3$ at 20°C). The total (experimental) deposition velocity, comprising contributions from both aerodynamic and liquid phase resistance, can be calculated from $v_D = Vk/A$, where V is the volume of the chamber (2 liters), k is the rate constant for removal of ozone (corrected for the small removal rate in the absence of *Laminaria*), and A is the area of the *Laminaria* strip (≈100 cm^2). The rate constant k for ozone removal in our experiments was 0.0115 s^{-1} (Fig. 3*b*), giving a total deposition velocity of ≈0.2 cm·s^{-1}. Using typical values of aerodynamic resistance r_a (15, 16), the deposition velocity due only to liquid phase diffusion and chemical reactions ($1/r_l$) is estimated to be in the range 0.25–1 cm·s^{-1}. This is only slightly lower than calculations based on 20 mM I^- present in the surface film of *Laminaria* of ≈7 cm·s^{-1}.

Theoretical Considerations About the Suitability of Iodide as Antioxidant. Tables S3 and S4 highlight that iodide is more favorable than chloride or bromide as a reductant with ROS.

Thermodynamic data (Table S3) show that $HO_2^{\bullet}$ and $OH^{\bullet}$ are one-electron oxidants that can, among the halides, only oxidize iodide. H_2O_2 and O_3 are favorable two-electron oxidants also for Br^- and Cl^-, with iodide being more favorable. Thermodynamic data, which are used to calculate one-electron transfer reactions (**1**–**7**) (17) and two-electron transfer reactions (**8**–**11**) (18) in Table S2, are from the literature using original ΔG_f and E^o data for each chemical species where $\Delta G = -n\,FE$. In reaction **9**, X^- transfers two electrons to form X^+ which then reacts with water to form HOX and H^+. Reaction **8** can be viewed as a two-electron transfer process where X^- transfers two electrons to form X^+, which then reacts with X^- to form X_2. At surface seawater pH (≈8), [X] (reactions **1**–**7**) is ½ X_2, which rapidly disproportionates to HOX and X^-. Haloperoxidases, which are abundant in the *Laminaria* apoplast (14, 19), enable the rapid halide-assisted disproportionation of hydrogen peroxide. In the absence of organic substrates, they would catalyze a cyclic, pseudocatalase reaction sequence.

Also with regard to kinetics, iodide is very well suited as an antioxidant (Table S4). Iodide reacts faster than bromide, chloride, glutathione, and ascorbate with ozone and singlet oxygen, respectively. Its rate constant for the reaction with hydroxyl radicals is in the same order of magnitude as those of ascorbate and glutathione, and triiodide reacts 3 orders of magnitude faster than glutathione and ascorbate. The reaction of iodide with hydrogen peroxide is slow nonenzymatically (even though within the same order of magnitude as that of ascorbate and glutathione, and still much faster than bromide and chloride). Again, it should be highlighted that haloperoxidases are very abundant in the *Laminaria* cell wall that catalyze the fast halide-assisted disproportionation of hydrogen peroxide (see above).

1. Luther GW, III, Swartz CB, Ullman WJ (1988) Direct determination of iodide in seawater by cathodic stripping square wave voltammetry. *Anal Chem* 60:1721–1724.
2. Herring JR, Liss PS (1974) A new method for the determination of iodine species in seawater. *Deep-Sea Res* 21:777–783.
3. Takayanagi K, Wong GTF (1986) The oxidation of iodide to iodate for the polarographic determination of total iodine in natural waters. *Talanta* 33:451–454.
4. Küpper FC, Kloareg B, Guern J, Potin P (2001) Oligoguluronates elicit an oxidative burst in the brown algal kelp *Laminaria digitata*. *Plant Physiol* 125:278–291.
5. Boneberg EM, Hareng L, Gantner F, Wendel A, Hartung T (2000) Human monocytes express functional receptors for granulocyte colony-stimulating factor that mediate suppression of monokines and interferon-gamma. *Blood* 95:270–276.
6. Tietze F (1969) Enzymic method for quantitative determination of nanogram amounts of total and oxidized glutathione: Applications to mammalian blood and other tissues. *Enz Anal Biochem* 27:502–522.
7. Foyer CH, Rowell J, Walker D (1983) Measurements of the ascorbate content of spinach leaf protoplasts and chloroplasts during illumination. *Planta* 157:239–244.
8. Feiters MC, Küpper FC, Meyer-Klaucke W (2005) X-ray absorption spectroscopic studies on model compounds for biological iodine and bromine. *J Synchrotron Radiat* 12:85–93.
9. Almeida M, Duarte C, Alexandre A, Humanes M, da Silva J (2001) Iodination of L-tyrosine by vanadium-dependent haloperoxidases. *J Inorg Biochem* 86:121–121.
10. Butler A (1998) Vanadium haloperoxidases. *Curr Opin Chem Biol* 2:279–285.
11. Butler A, Carter JN, Simpson MT (2001) in *Handbook on Metalloproteins*, eds Bertini I, Sigel A, Sigel H (Dekker, New York).
12. Carpenter LJ, Malin G, Küpper FC, Liss PS (2000) Novel biogenic iodine-containing trihalomethanes and other short-lived halocarbons in the coastal East Atlantic. *Global Biogeochem Cycles* 14:1191–1204.
13. Palmer CJ, Anders TL, Carpenter LJ, Küpper FC, McFiggans GB (2005) Iodine and halocarbon response of *Laminaria digitata* to oxidative stress and links to atmospheric new particle production. *Environ Chem* 2:282–290.
14. Küpper FC, *et al.* (1998) Iodine uptake in Laminariales involves extracellular, haloperoxidase-mediated oxidation of iodide. *Planta* 207:163–171.
15. Garland JA, Elzerman AW, Penkett SA (1980) The mechanism for dry deposition of ozone to seawater surfaces. *J Geophys Res* 85:7488–7492.
16. Jones CE (2006) Aqueous chemistry and photochemistry of volatile organic iodine in sea water. PhD thesis (Univ of York, York, UK).
17. Stanbury DM (1989) in *Advances in Inorganic Chemistry*, ed Sykes AG (Academic, Orlando, FL), pp 167–211.
18. Stumm W, Morgan JJ (1996) *Aquatic Chemistry* (Wiley, New York).
19. Colin C, *et al.* (2003) The brown algal kelp *Laminaria digitata* features distinct bromoperoxidase and iodoperoxidase activities. *J Biol Chem* 278:23545–23552.

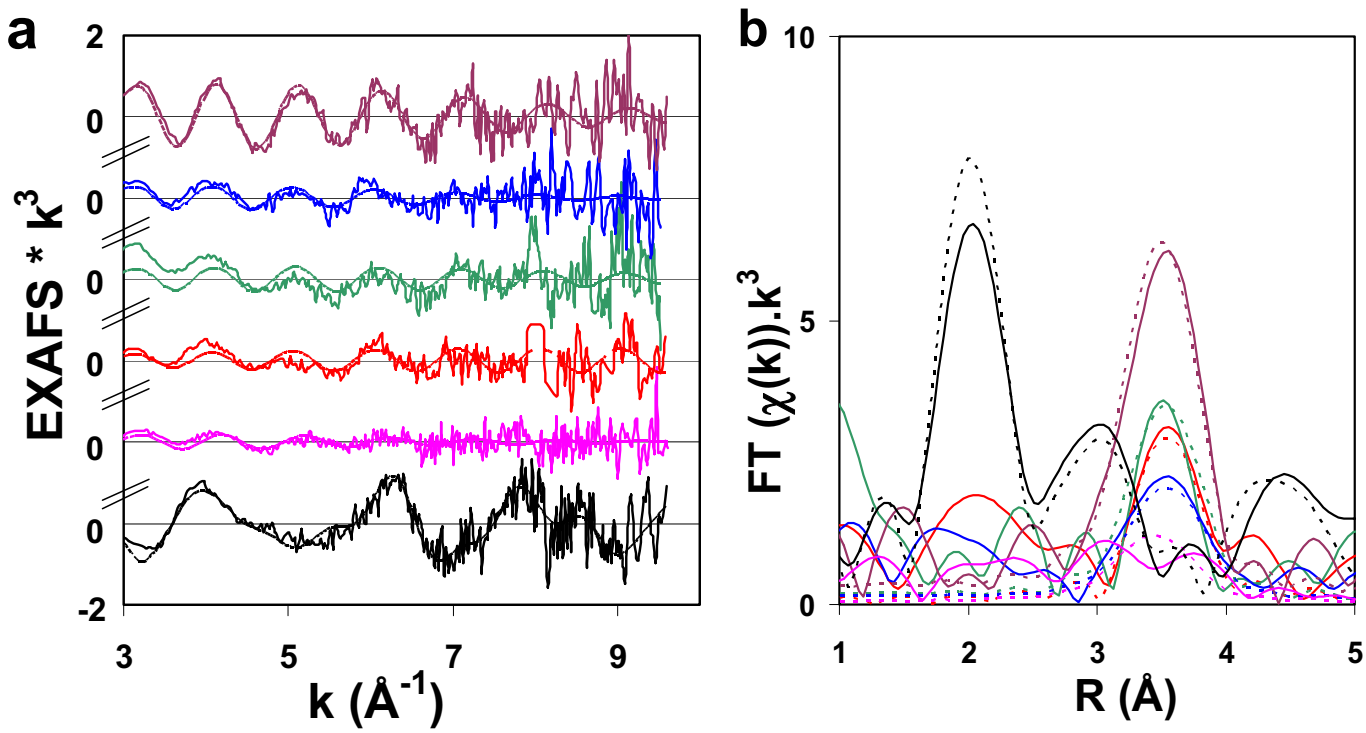

Fig. S1. k^3-weighted K-edge EXAFS (*a*) and the corresponding, phase-corrected Fourier transform (*b*) of *Laminaria digitata* tissues (cf. Fig. 1). Solid lines, experimental; dashed lines, simulations; black, lyophilized *Laminaria* rehydrated in seawater with 2 mM H_2O_2 [simulation: 1.0 phenyl at 2.1 Å, $a = 0.003$ (*a*, Debye–Waller-type factor as $2\sigma^2$ in Å^2)]; pink, lyophilized *Laminaria* (2.2 O at 3.51 Å, $a = 0.038$ Å^2); red, fresh *Laminaria* (1.6 O at 3.58 Å, $a = 0.005$ Å^2); plum, 20 mM NaI [simulation: 10.0 O at 3.56 Å, $a = 0.034$ Å^2 (*a*, Debye–Waller-type factor as $2\sigma^2$ in Å^2)].

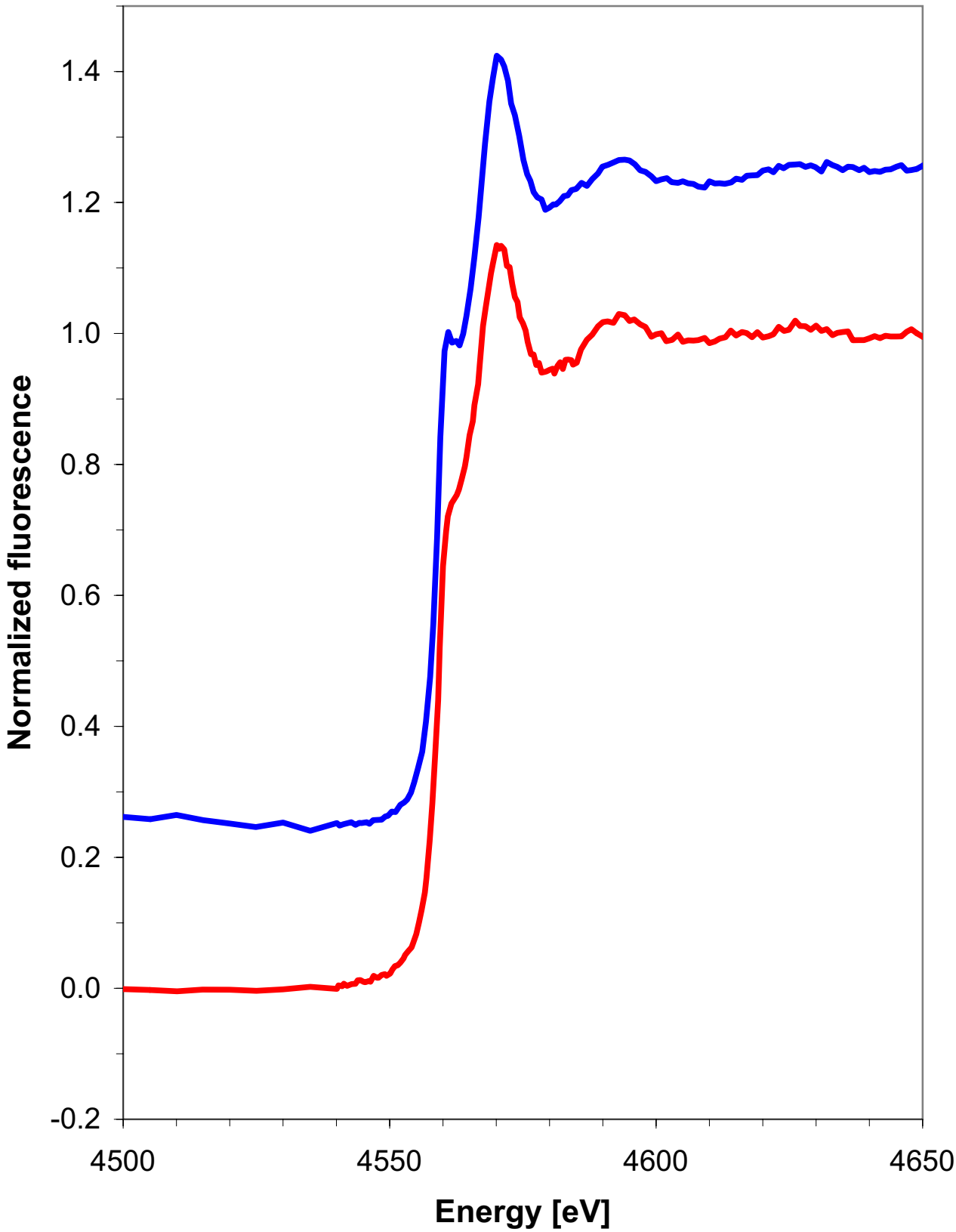

Fig. S2. L_3-edge XAS of 10 mM aqueous NaI (red) and fresh *Laminaria digitata* tissues (blue). Both spectra differ considerably from the edge pattern of other iodine-containing model compounds (I_2, $NaIO_3$, $NaIO_4$, iodotyrosine, CHI_3, IBr, CI_4; not shown).

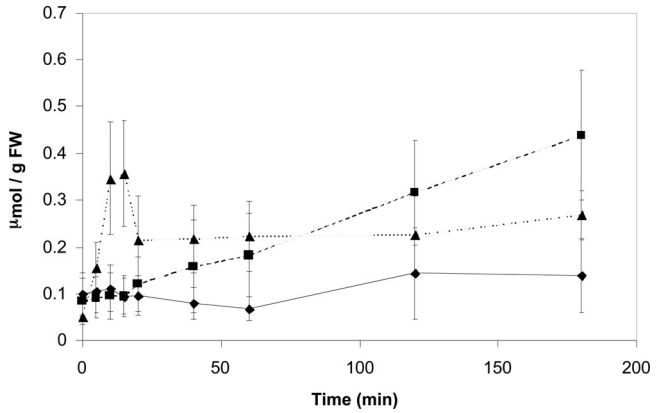

Fig. S3. Efflux of iodine from ^{125}I-charged *L. digitata* sporophytes following oxidative stress starting at $t = 0$ min, induced by 150 μg·ml^{-1} oligoguluronate (squares) or 2 mM H_2O_2 (triangles; control without additions shown as diamonds).

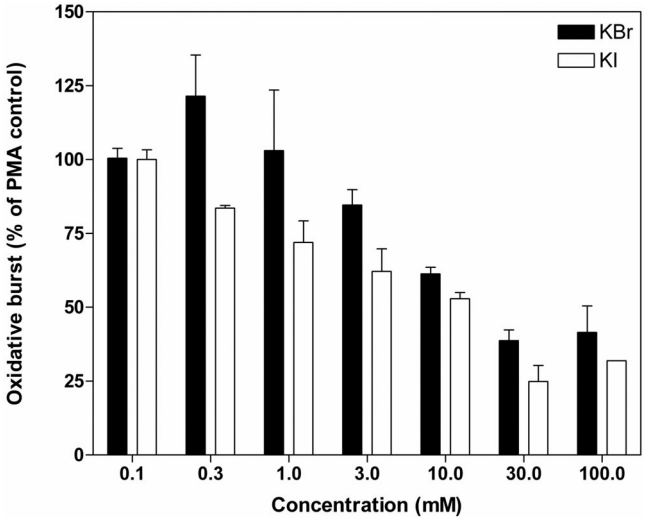

Fig. S4. Whole-blood assay to determine the effect of iodide and bromide on the oxidative burst of leukocytes. Whole blood was preincubated for 30 min at 37°C with different concentrations of KI or KBr. Then, leukocytes were stimulated with 2 μg·ml^{-1} phorbol 12-myristate 13-acetate for 5 min at 37°C. The amount of H_2O_2 formed was determined calorimetrically in the cell-free supernatants of the blood samples.

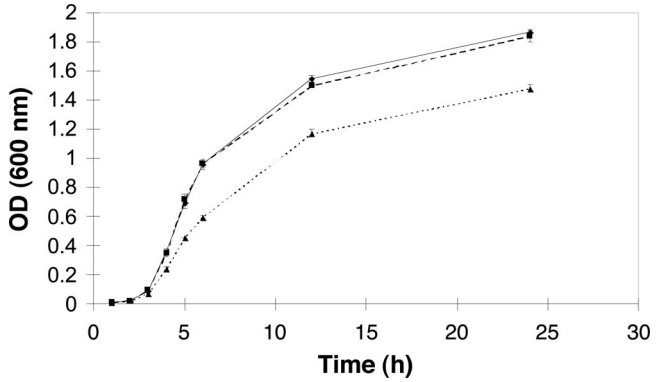

Fig. S5. Time course of the optical density (at 600 nm) of a growth experiment with the kelp-epiphytic bacterial strain Ldm 2 in the presence of various iodide concentrations (control, diamonds; 10 mM KI, squares; 100 mM KI, triangles; 10 μM, 100 μM, and 1 mM, not shown).

Table S1. Parameters with fitting errors for the simulations of the EXAFS of iodine in *Laminaria* tissues and model compounds (distances to iodine in Å, Debye–Waller-type factors as 2 s^2 in $Å^2$ in parentheses)

Parameter	Aqueous NaI (20 mM)	Unstressed *Laminaria*	Freeze-dried *Laminaria*	Freeze-dried *Laminaria*, after re-hydration with 2 mM H_2O_2
Δ*EF*, eV	−7.7 ± 1.4	−8.7 ± 0.7	−6.1 ± 0.5	−6.6 ± 0.9
Energy range, eV	20–350	20–350	20–350	20–350*
O	9.1 ± 2.5 at 3.56 ± 0.02 (0.031 ± 0.009)	1.6 ± 0.2 at 3.588 ± 0.007 (0.005 ± 0.002)	2.2 ± 0.1 at 3.51 ± 0.01 (0.038 ± 0.001)	
C (phenyl)				1.0 ± 0.1 at 2.094 ± 0.006 (0.003 ± 0.001)
Fit index (k^3-weighting) × 10^3	0.6732	0.5566	1.287	0.2141

The fitting errors do not exceed the systematic errors for EXAFS, viz. 0.003 and 20% for first shell distances and occupancies, respectively.

*For this sample, the oscillations can be simulated over a longer energy range (18–650 eV), giving virtually the same result [1.0 ± 0.1 C (phenyl) at 2.093 ± 0.006 Å (0.007 ± 0.002 $Å^2$) with a fit index × 10^3 of 0.2141].

Table S2. Molecular iodine production rate, iodocarbon production rate (mean value of CH_3I, C_2H_5I, 1-C_3H_7I, 2-C_3H_7I, CH_2ICl, and CH_2I_2), and particle numbers in ozone scavenging experiments with *Laminaria* thalli

I_2, pmol·min^{-1}·g FW^{-1}	Particles, g FW^{-1}
1.01	1.59×10^7
2.93	3.98×10^5
3.29	1.79×10^4
9.29	4.75×10^5
15.16	1.73×10^9
130.00	3.75×10^{10}

Mean TIC, pmol·min^{-1}·g FW^{-1}	Particles, g FW^{-1}
0	5.14×10^3
0.9	0
1.32	0
1.66	2.91×10^4
1.8	4.02×10^7
1.9	1.08×10^8
2.219	4.0×10^1
2.242	1.09×10^3
2.26	1.10×10^3
2.357	5.35×10^6
2.411	2.62×10^6
2.859	4.29×10^2
3.348	2.30×10^2
4.327	7.05×10^3
5.409	2.11×10^5

There is a strong correlation ($r^2 = 0.9953$) between the formation of molecular iodine and particle production (*Upper*). In contrast, there is no correlation ($r^2 = 0.0341$) between total iodocarbon concentrations vs. particles (*Lower*).

Table S3. Thermodynamic calculations for one- and two-electron transfer reactions of halides with oxygen species (triplet and singlet oxygen, hydroxyl radical, superoxide, hydrogen peroxide, and ozone) at standard conditions

	ΔG_R, kJ·mol^{-1}		
	Cl^-	Br^-	I^-
One-electron transfer per X^-			
[1] $X^- + {}^3O_2 \rightarrow [X] + O_2^{\bullet -}$	247.97	200.7	143.76
[2] $X^- + OH^{\bullet}_{(g)} \rightarrow [X] + OH^-$	49.21	1.93	−55.0
[3] $X^- + OH^{\bullet}_{(aq)} \rightarrow [X] + OH^-$	67.54	20.26	−36.66
[4] $X^- + {}^1O_2 \rightarrow [X] + O_2^{\bullet -}$	152.45	105.17	48.24
[5] $X^- + H_2O_2 \rightarrow [X] + OH^{\bullet} + OH^-$	235.42	188.15	131.22
[6] $X^- + H^+ + HO_2^{\bullet} \rightarrow [X] + H_2O_2$	93.59	46.31	−10.61
[7] $X^- + O_3 \rightarrow [X] + O_3^{\bullet -}$	135.08	87.80	30.87
Two-electron transfer per X^-			
[8] $2\,X^- + H^+ + O_3 \rightarrow X_2 + O_2 + OH^-$	−57.9	−112.5	−217.3
[9] $X^- + H^+ + O_3 \rightarrow HOX + O_2$	−111.8	−141.4	−210.8
[10] $X^- + H^+ + {}^1O_2 + H_2O \rightarrow HOX + H_2O_2$	62.48	32.88	−36.43
[11] $2\,X^- + 2\,H^+ + {}^1O_2 \rightarrow X_2 + H_2O_2$	96.66	42.06	−62.76
[12] $X^- + H_2O_2 \rightarrow HOX + OH^-$	28.21	−1.39	−70.81
[13] $2\,X^- + 2\,H^+ + H_2O_2 \rightarrow X_2 + 2\,H_2O$	−77.66	−132.26	−237.08

Numbers in boldface type indicate that the reactions are favorable and that iodide is the easiest halide to oxidize (reactions **2**, **3**, **6**, and **8**–**11**).

Table S4. Rate constants for the reactions of ozone, singlet oxygen, hydroxyl radicals superoxide, and hydrogen peroxide with halides, glutathione, and ascorbate, respectively

Compound	k_{12}, $M^{-1}\cdot s^{-1}$	Ref.
	O_3 reactions with	
I^-	1.2×10^9	1
Br^-	2.48×10^2	1
Cl^-	$<3 \times 10^{-3}$	2
Ascorbate	4.8×10^7	3
Glutathione	2.5×10^6	3
	Singlet oxygen ($^1O_2$) reactions with	
I^-	1×10^8	4 (aprotic solvents)
	8.7×10^5	5, p. 896 (pH ~ 7)
Br^-	1.0×10^3	5, p.895 (in D_2O)
Cl^-	1.0×10^3	5, p.895 (in D_2O)
Ascorbate	8.3×10^6	5, p. 904 (pH 6.8)
Glutathione	2.4×10^6	5, p. 883 (in D_2O, 310 K, pD 7.4)
	OH radical (· OH) reactions with	
I^-	1.2×10^{10}	6, p. 527
Ascorbate	1.1×10^{10}	6, p. 700
Glutathione	1.3×10^{10}	6, p. 723 (pH 5.5)
Dimethyl sulfoniopropionate	3×10^8	7
Dimethyl sulfide	1.9×10^{10}	6
Dimethyl sulfoxide	6.6×10^9	6
	Superoxide (O_2^-) reactions with	
I_3^-	1×10^8	8, p. 1063 (no data available for I^-)
Ascorbate	2.7×10^5	8, p. 1069 (pH 7.4)
Glutathione	2.4×10^5	8, p. 1075 (pH 7.8)
	Hydrogen peroxide (H_2O_2) reactions with	
I^-	0.69	9
Br^-	2.3×10^{-5}	9
Cl^-	1.1×10^{-7}	9
Ascorbate	2×10^0	10
Glutathione	$2–20 \times 10^0$	11
Glutathione peroxidase	6×10^7	12

1. Liu Q, *et al.* (2001) Kinetics and mechanisms of aqueous ozone reactions with bromide, sulfite, hydrogen sulfite, iodide, and nitrite ions. *Inorg Chem* 40:4436–4442.
2. Hoigné J, Bader H, Haag WR, Staehelin J (1985) Rate constants of reactions of ozone with organic and inorganic compounds in water—III. Inorganic compounds and radicals. *Water Res* 19:993–1004.
3. Kanofsky JR, Sima PD (1995) Reactive absorption of ozone by aqueous biomolecule solutions—Implications for the role of sulfhydryl compounds as targets for ozone. *Arch Biochem Biophys* 315:52–62.
4. Rosenthal I, Frimer A (1976) The quenching effect of iodide ion on singlet oxygen. *Photochem Photobiol* 23:209–211.
5. Wilkinson F, Helman WP, Ross AB (1995) Rate constants for the decay and reactions of the lowest electronically excited singlet state of molecular oxygen in solution. An expanded and revised compilation. *J Phys Chem Ref Data* 24:663–1023.
6. Buxton GV, Greenstock CL, Helman WP, Ross AB (1988) Critical review of rate constants for reactions of hydrated electrons, hydrogen atoms and hydroxyl radicals in aqueous solution. *J Phys Chem Ref Data* 17:513–886.
7. Sunda W, Kieber DJ, Kiene RP, Huntsman S (2002) An antioxidant function for DMSP and DMS in marine algae. *Nature* 418:317–320.
8. Bielski BHJ, Cabelli DE, Arudi RL, Ross AB (1985) Reactivity of HO_2/O_2^- radicals in aqueous solution. *J Phys Chem Ref Data* 14:1041–1100.
9. Mohammed A, Liebhafsky HA (1934) The kinetics of the reduction of hydrogen peroxide by the halides. *J Am Chem Soc* 56:1680–1685.
10. Polle A, Junkermann W (1996) Inhibition of apoplastic and symplastic peroxidase activity from Norway spruce by the photooxidant hydroxymethyl hydroperoxide. *Plant Physiol* 104:617–623.
11. D'Autréaux B, Toledano MB (2007) ROS as signalling molecules: Mechanisms that generate specificity in ROS homeostasis. *Nat Rev Mol Cell Biol* 8:813–824.
12. Flohe L, Loschen G, Günzler WA, Eichele E (1972) Glutathione peroxidase. V. The kinetic mechanism. *Hoppe-Seyler's Z Physiol Chem* 353:987–999.

Table S5. Carbon–halogen (C–X) bond length, bond dissociation energies, and relative reactivity in halomethanes [CH_3–X] [McMurry J (1984) in *Organic Chemistry* (Cole, Belmont, CA), Tables 9.2 and 10.15]

	Bond length, pm	Bond dissociation energy, kJ·mol^{-1}	Relative reactivity to hydroxide (defined as 0)
C–F	139	456	1
C–Cl	178	351	200
C–Br	193	293	10,000
C–I	214	234	30,000

Taken together, these data show that the C–I bond provides an excellent leaving group in substitution reactions.